

# The Recognition of Unusual Objects in the Sloan Digital Sky Survey Color System

Kevin Krisciunas, Bruce Margon, and Paula Szkody

Department of Astronomy, University of Washington, Box 351580, Seattle, WA 98195–1580

Electronic mail: kevin, margon, szkody@astro.washington.edu

Received \_\_\_\_\_; accepted \_\_\_\_\_

## ABSTRACT

We present 5 filter photometry of 21 carbon stars, 15 asteroids, 15 cataclysmic variables, 6 metal-poor stars, 5 Cepheids, 1775 field stars, blue horizontal branch (BHB) stars and RR Lyrae stars in the globular clusters M 15 and M 2, two primary standards, and 19 secondary standards. The photometry was carried out using a filter set identical to that which will be used for the Sloan Digital Sky Survey. We find that carbon stars, CVs, R-type, J-type, and V-type asteroids, BHB stars, and RR Lyr stars should be identifiable on the basis of SDSS photometry alone, while Cepheids, metal-poor stars, and many types of asteroids are indistinguishable from the stellar locus of field stars.

*Subject headings:* Sloan Digital Sky Survey, photometry, carbon stars, asteroids, cataclysmic variables, Cepheids, RR Lyrae stars, metal-poor stars, horizontal branch stars

## 1. Introduction

The Sloan Digital Sky Survey (SDSS) will image  $10^4 \text{ deg}^2$  of the northern high-latitude sky to approximately magnitude 23 in five special filter bands from roughly 3500 to 9000 Å (Gunn & Knapp 1993; Gunn & Weinberg 1995; Margon 1998). The broad-band filters of the SDSS system cover the full wavelength range of an optical CCD. The bandpasses overlap very little, thus allowing essentially unique portions of an object’s spectral energy distribution to be sampled by each filter. Furthermore, sky features such as the 5460 Å Hg I line, the 5577 Å line of [O I] and a strong OH band fall between the bandpasses, thus allowing more accurate photometry because one is not so much at the mercy of short-term changes of the sky brightness. The resulting magnitudes will be on the AB system, referred to a spectrum with constant  $f_\nu$  (rather than an A0 V star), and represent the fluxes a flat spectrum source with a given  $V$  magnitude would have near the effective wavelengths of the filters.

The resulting SDSS photometry of roughly  $10^8$  objects (stars, galaxies, quasars, etc.) will be used to select targets for multifiber spectroscopy, as well as constitute a permanent archive for a large variety of astrophysical problems. For both of these functions, it is imperative to understand whether (and how) interesting subclasses of objects stand out compared to the normal stellar locus in multi-color space. Further, the precise transformation between the SDSS color system and more traditional ones will become very important for a variety of future studies.

Although the exact SDSS photometric system requires use of the actual survey telescopes, cameras, and filters, it is already possible to mimic the system reasonably well. The names of the Survey bandpasses are  $u'$ ,  $g'$ ,  $r'$ ,  $i'$ , and  $z'$ , and their effective wavelengths (Fukugita et al. 1996, hereafter F96) are 3557, 4825, 6161, 7672, and 9097 Å, respectively. While the photometric filter profiles and CCD characteristics of SDSS photometry have

been defined, a fully calibrated set of photometric standards is still being established. We therefore follow the example of Richards et al. (1997) and refer to our observations, as  $u^*$  data,  $g^*$  data, etc.

The observations and analysis of this paper have several purposes: (1) to quantify the effectiveness of the SDSS filters for isolating unusual classes of objects from the normal stellar locus; (2) to complement previous work and further the determination of the stellar locus of normal stars in the four Sloan colors;<sup>1</sup> and (3) to determine the magnitudes and colors of a list of potential secondary standard stars, which will aid further SDSS observations and contribute to the establishment of the Sloan system.

Richards et al. (1997) and Newberg et al. (1997) have used the SDSS Monitor Telescope at Apache Point Observatory (New Mexico) and the 1-m telescope of the United States Naval Observatory (USNO) to delineate the locus of field stars and the positions of quasars in SDSS multi-color space. Our observations here on a larger number of fields (but typically to shallower photometric depth) confirm the position of the stellar locus. We present observations of carbon stars, cataclysmic variables (CVs), asteroids, some metal-poor stars, and some globular cluster stars of interest (Cepheids, RR Lyrae stars, and horizontal branch stars). While the exact photometric values of our observations will change once the official SDSS calibration is established, we believe that the observations presented here will require relatively small corrections. The *qualitative* results should be unchanged, since objects that separate from the stellar locus *now* will still separate from the stellar locus, no matter how the “sausage” is twisted in multi-color space by the final calibration.

---

<sup>1</sup>In addition to the observational papers cited above on this problem, Lenz et al. (1998) present extensive synthetic photometry which is also relevant.

## 2. Observations and Data Reduction

### 2.1. Techniques

Our observations were obtained using the USNO 1-m Ritchey-Chrétien reflector in Flagstaff, Arizona. The camera contains an  $\text{LN}_2$  cooled  $1024 \times 1024$  charge-coupled device (CCD). The gain is  $\approx 7$  electrons per analog-to-digital unit (ADU), with a read noise of 6 electrons. The plate scale is  $0.68 \text{ arcsec pixel}^{-1}$ , giving a field of view of  $11.5 \times 11.5$  arcmin. Since non-linear effects begin at  $\approx 16,000$  ADUs, we occasionally had to obtain extra, shorter, exposures on some bright stars, or defocus the camera slightly if the required exposure would have to have been less than 4 seconds.

The USNO camera contains a UV-enhanced CCD nearly identical to the  $u'$  CCDs on the SDSS 2.5-m telescope. The *other* four bands of the camera on the 2.5-m telescope do not use UV-enhanced chips. The effective wavelengths for the other four filters used for the observations presented in this paper are thus slightly different than the values given by F96. The smaller SDSS monitor telescope will also use a single UV-enhanced CCD to define the SDSS system.

One of the major drawbacks of the USNO 1-m telescope, which was originally completed in 1934, is that one typically cannot accurately guide the telescope when pointed at an object further than two hours from the meridian. Thus, to observe standards at a wide range of air mass requires that some of the standards be rather far south. On some nights we did observe some stars twice, at air masses  $\approx 1.2$  and  $\approx 1.8$ , thus allowing zeroth order estimates of the extinction in each filter. We did not obtain sufficient data on red-blue pairs of stars to derive the *second* order atmospheric coefficients according to the standard method described by Hardie (1962). Thus we performed only first order atmospheric corrections.

Altogether we observed on 9 nights from UT dates 27 September to 5 October 1997. Nights 2, 3, 4, 8, and 9 were photometric from start to finish. Half of nights 1, 5, and 7 were good, as was the end of night 6. We took care to use only data bracketed by consistent standards, indicating which portions of the partial nights were indeed perfectly clear. We observed the SDSS primary standard BD +17° 4708 on nights 1, 3, 4, 8, and 9. BD +21° 607, which is intended to become a primary standard, was observed on nights 2, 7, and 8.

In addition to the primary standards, we observed 19 secondary standards from a list drawn up for the Sloan project (Allyn Smith, private communication). These are mostly standards of Landolt (1992) – stars known to be constant in brightness and with known Johnson UBV and Cousins RI magnitudes. On full nights we obtained between 14 and 19 sets of 5 filter standards data.

Except for the globular cluster data, we reduced all our data with the IRAF data reduction package. This first involved subtracting the bias frames, constructing sky flats with the median of three sky frames per filter per night, then flattening and trimming the frames. For the data on stars and asteroids we determined the instrumental magnitudes as aperture magnitudes, using **phot** within the **apphot** package. We almost always used an aperture radius of 6 pixels. This was after the inspection of many stars in many frames using **imexam**. For sets of frames we selected the field stars to be reduced using **daofind**. Our selection criterion was  $10\sigma$  over sky in the  $u^*$  filter. This was because we wanted to maximize the number of stars detected in all 5 filters, and the  $u^*$  filter plus the near-UV quantum efficiency of the CCD gives the least efficient response. Calibration of the data was done within the **photcal** package, in particular with **mknoobsfile**, **fitparams**, and **evalfit**.

The derivation of a table of standard star magnitudes and colors was a time consuming, iterative, but convergent process. The values in A. Smith’s list of Sloan secondary standards were generated for the purpose of estimating exposure times, not for the purpose of data

reduction. But given the hour angle constraints of the telescope mentioned above, we needed *some* set of values for the derivation of atmospheric extinction and atmospheric reddening if we could not observe the same stars at a range of air mass. We therefore temporarily adopted the predicted  $r^*$  magnitudes and four colors for the stars and adjusted these values until: (1) we obtained sensibly linear photometric solutions; and (2) the RMS internal errors of the fits on photometric nights were smaller than 0.02 mag. By “sensible linear photometric solution” we mean the following. We obtained instrumental magnitudes in each of the 5 SDSS filters. To obtain  $r^*$  magnitudes let us designate the instrumental  $r^*$  and  $i^*$  magnitudes by  $r_{instr}$  and  $i_{instr}$ , the mean air mass over the course of the  $r^*$  exposure by  $\overline{X_r}$ , and the first order  $r^*$ -band extinction by  $k_r$ . We have:

$$r^* = ZP_r + r_{instr} - k_r \overline{X_r} + c_r (r_{instr} - i_{instr}),$$

where  $ZP_r$  is the zero point and  $c_r$  is a scaling coefficient. Of course, we could have just as easily used the instrumental  $g^*-r^*$  color in the previous equation. For the reduction of  $r^*-i^*$  colors we have an equation such as:

$$r^* - i^* = ZP_{ri} - k_{ri} \overline{X_{ri}} + c_{ri} (r_{instr} - i_{instr}),$$

where  $ZP_{ri}$  is the zero point,  $k_{ri}$  is the first order atmospheric reddening, and  $c_{ri}$  is a scaling coefficient. There are, of course, analogous expressions for the other three SDSS colors.

If we were to include second order terms, in the first equation we would use a slightly different first order extinction term, say  $k'_r$ , and we would have to add a term such as  $k''_r \overline{X_{ri}} (r_{instr} - i_{instr})$ . The  $r^*-i^*$  color reduction equation would require, instead, a first order term such as  $k'_{ri}$  and would require the addition of a term such as  $k''_{ri} \overline{X_{ri}} (r_{instr} - i_{instr})$ . There would be analogous expressions for other SDSS colors. While F96 gives estimates for the second order terms, we decided to set them to zero. F96 suggests that the largest second

order term is for  $u^*-g^*$  reductions for stars with  $u^*-g^*$  bluer than +1.3. For those stars the inclusion of a second order term would add at most a few hundredths of a magnitude to the scatter of the data. For stars with  $u^*-g^*$  redder than +1.3, such as our carbon stars, some of which are very red indeed, F96 suggests that the second order color term for  $u^*-g^*$  reductions is exactly 0.00, in which case we may be able to take at face value the derived  $u^*-g^*$  colors of the reddest stars presented here.

We discovered that it is possible to construct a table of secondary standards that gives sensible extinction and atmospheric reddening, low RMS internal errors for the nightly fits, and which gives the right values for BD +17° 4708, but which does *not* give  $c_r = 0.00$ , or  $c_{ug}, c_{gr}, c_{ri}, c_{iz} = 1.00$ . This would be a photometric “system”, but not a system that would allow the Sloan magnitudes to be converted to AB magnitudes for stars with colors *other than* those close to the colors of BD +17° 4708.

Because the SDSS standard star network is still incomplete, conventional photometric reduction procedures, including the use of color terms, are not appropriate. For those wholly photometric nights when BD +17° 4708 was observed, we determined the “standardized values” for the secondary standards by means of single filter differential photometry with respect to this primary, using first order extinction corrections, then adding the differential values to the values of primary (which are known from spectrophotometry). This gave a new standards table, which we then tested with IRAF. The nightly solutions gave nearly the same extinction and atmospheric reddening values as those used to derive the magnitudes and colors of the secondary stars. Within IRAF the resulting color coefficients used to scale instrumental magnitudes and colors were, within very small errors, equal to 0.00 for the  $r^*$ -band data, and 1.00 for the four colors. Arithmetically, this is the same as simply correcting the instrumental magnitudes (or colors) of the program objects and field stars to outside-the-atmosphere values with first order atmospheric terms.

We derived the zero points and first order extinction and atmospheric reddening parameters using as much information as the 9 night observing run provided – as many as two primary and 17 secondary standards per night. This is better than deriving the nightly zero points solely on the basis of one star, no matter how primary it is. It could have been the case that we were observing through thin cirrus only at the time we were measuring the primary standard.

As an example of the success of our photometric method, we show in Fig. 1 a plot of the  $u^*-g^*$  photometric solution for the night of 29 September 1997, using a first order atmospheric reddening term of  $k_{ug} = 0.26$  mag/air mass. The  $y$ -intercept is the photometric zero point for this night for this color index; it is not zero because of the different bandpass widths of the  $u^*$  and  $g^*$  filters and the variation of quantum efficiency of the chip as a function of wavelength. The slope of the line is statistically indistinguishable from 1.00, and the RMS residual of the fit is a remarkably low  $\pm 0.010$  mag. Other photometric solutions (i. e. different colors and different nights) are very similar to Fig. 1, if appropriate atmospheric terms are used. This means that our primary standard and secondary standards are self-consistent, and we believe will closely approximate the eventual, official SDSS system.

Based on 6 nights of observations at the USNO Flagstaff site, on which we observed an adequate number of standards under clear skies and over a wide enough air mass range, we find a mean first order  $r^*$ -band extinction of  $k_r = 0.109 \pm 0.018$  mag/air mass. We find mean atmospheric reddening values (in the same units) of  $k_{ug} = 0.292 \pm 0.043$ ,  $k_{gr} = 0.083 \pm 0.008$ ,  $k_{ri} = 0.067 \pm 0.017$ , and  $k_{iz} = -0.013 \pm 0.018$ .<sup>2</sup> For comparison, F96 give

---

<sup>2</sup> $k_{iz} < 0$  implies that the  $z^*$ -band extinction was greater than the  $i^*$ -band extinction. Since near-infrared extinction is dominated by water vapor emission, not scattering by aerosols, it is physically reasonable that  $k_{iz}$  can be negative. See Fig. 1 of Krisciunas et al. (1987).

predictions for Apache Point of  $k_r = 0.092$ ,  $k_{ug} \approx 0.38$ ,  $k_{gr} = 0.090$ ,  $k_{ri} = 0.013$ , and  $k_{iz} = -0.032$  mag/air mass.

In Table 1 we give  $r^*$  magnitudes and four colors of two primary standards and 19 secondary standards, with the values rounded off to the nearest hundredth. In most cases the measurements match, to better than a hundredth, those derived filter by filter on the four whole nights when BD +17° 4708 was observed. In some cases we have adjusted the values by 0.01 or 0.02 mag by taking into account observations made over the course of the whole observing run. More observations of these stars would certainly be welcome, and redder standards must be added to the list.

F96 predicts transformations between the Johnson UBV and Cousins RI systems and the SDSS system. We find similar, but not identical, transformations from actual observations of real stars, and suggest that the following equations be used:

$$r^* = V - 0.42 (B - V) + 0.10 ,$$

$$u^* - g^* = 1.33 (U - B) + 1.18 ,$$

$$g^* - r^* = 0.96 (B - V) - 0.18 ,$$

$$r^* - i^* = 0.99 (R - I) - 0.22 ,$$

$$i^* - z^* = 0.67 (R - I) - 0.19 .$$

F96 gives two transformations between R–I and  $r^*-i^*$ , depending on whether R–I is less than or greater than +1.15. Since our reddest standard has R–I = 0.81, we can

only consider one of the transformations. These transformations will probably change yet again when the final SDSS photometry calibration is determined. For now it seems more sensible to use our transformations, based on actual data, rather than use the predicted transformations given in F96.

In Tables 2, 3, and 4 we give photometric results for cataclysmic variables, carbon stars, and asteroids, respectively. For the most part we do not state the internal errors of the points, as they are often less than  $\pm 0.01$  mag, and very rarely larger than  $\pm 0.02$  mag.

## 2.2. Cataclysmic Variables

Since CVs occupy some of the same color phase space as quasars, we wish to see how well SDSS filters will differentiate them from each other. In Table 2 we give the CV types, the orbital periods, and the nightly means of  $r^*$  and four colors for 15 CVs. The CVs were selected to cover a range of orbital periods, magnetic field strengths, and mass transfer rates, all of which affect the colors. CVs which have long orbital periods, or which are in low mass transfer states, usually show the secondary star, so they will be redder. Large magnetic fields can result in red cyclotron emission, and large mass transfer rates lead to steady state disks which dominate the emission, yielding a flux distribution that is proportional to  $\lambda^{-2.3}$  (Warner 1995).

Because the dwarf novae undergo outbursts, and nova-like systems undergo high and low states of mass transfer, it is fortuitous that the objects were observed at various states. The dwarf novae AR And, V1159 Ori, and RX And were near outburst. (RX And was observed on four nights as it cooled and faded toward quiescence.) The disk nova-like system TT Ari was in a high state while the magnetic system AM Her was in a low state.

### 2.3. Carbon Stars

It is one of many stellar astronomy goals of SDSS systematically to discover significant numbers of faint high latitude carbon stars (FHLCS) (Totten & Irwin 1998), which are rare but interesting objects for multiple reasons. The most extreme examples (Margon et al. 1984) are at galactocentric distances of up to 100 kpc, and thus almost surely well beyond the dark matter halo. Such objects are thus crucial dynamical probes, and their sharp bandheads make accurate spectroscopic velocity determinations straightforward. Some uncertain but probably small fraction of FHLCS are in fact nearby dwarfs (Green & Margon 1994, Green 1998). Although only a dozen such objects are currently known, all are within  $\sim 100$  pc, and thus it seems certain that the until-recently unrecognized class of dC stars are by a large factor the numerically most common carbon stars in the Galaxy, overwhelming the well-studied C giants.

We selected more than 20 FHLCS stars for observation, primarily from the lists of Bothun et al. (1991), Sanduleak & Pesch (1988), and Slettebak, Keenan & Brundage (1969). Unfortunately only two dC stars were available during this observing run, although they have the virtue of including two of the brightest known objects, including the prototype, viz. G77-61 and LHS 1075.

In Table 3 we give our averaged data for 19 “regular” carbon stars and two dwarf carbon stars. Many of these stars are probably variable in brightness to some degree. For example, according the 4th edition of the *General Catalogue of Variable Stars* (Kholopov 1987), AM Scl irregularly varies between magnitude 12.42 and 13.29. For those few stars in Table 3 which were observed on more than one night, we see no evidence of variability.

## 2.4. Asteroids

We are interested to know if asteroids of different taxonomic types (Tholen & Barucci 1989) separate from the stellar locus in SDSS multi-color space; or, will SDSS photometry at least allow us to differentiate different types of asteroids from each other?

We observed 15 asteroids of 5 taxonomic types. In Table 4 we give nightly averages of the photometry. Three of the asteroids were observed on more than one night. Because asteroids can be variable in brightness and color, we do not average the data from more than one night.

The taxonomic types given in Table 4 are from Xu et al. (1995), with two exceptions. For 371 Bohemia, Xu et al. give its type as S. This object is now classed AS, meaning “olivine-rich S-type with near infrared absorption band minimum typically falling past 1 micron” (Hammergren, personal communication). The near-Earth asteroid 433 Eros is an S-type asteroid (Lee et al. 1996).

## 2.5. Metal-Poor Stars and Cluster Variables

In Table 5 we give photometry of six metal-poor stars, four Cepheids in M 2, and one Cepheid in M 15. The globular cluster data were reduced using Dophot version 2.0 (Schechter, Mateo, & Saha 1993), along with some notes from the Canary Islands Winter School (Mateo 1996). This code uses point spread function (PSF) fitting, a must when trying to reduce data in crowded stellar fields. From aperture photometry, reduced with IRAF, of stars in more empty parts of the M2 and M 15 frames, we were able to put the Dophot results on the same photometric system as our standard stars, with estimated systematic errors of 0.03 mag or less.

### 3. Discussion

In Figures 2, 3, and 4 we show our program objects (CVs, carbon stars, asteroids, metal-poor stars, and Cepheids) in color-color space. In Figures 5, 6, and 7 we add the locus of field stars.

Let  $\sigma_a$  and  $\sigma_b$  be the internal errors of the magnitudes of a star in filters  $a$  and  $b$ , respectively, and let  $\sigma_{ab} = \sqrt{(\sigma_a^2 + \sigma_b^2)}$ . In our color-color plots the field stars are only plotted if the corresponding value of  $\sigma_{ab}$  is less than 0.10 mag. While this reduces the number of stars in our field star sample, it sharpens the edges of the field star locus in multi-color space.

The stellar locus was derived from roughly 80 fields at a wide variety of galactic latitudes, and amounts to 1775 stars selected on the basis of their instrumental  $u^*$  counts to be at least  $10\sigma$  times the sky noise, with the criterion on internal errors mentioned above. In Fig. 5 we have included quasars observed by Richards et al. (1997), which have redshifts ranging  $0.06 < z < 2.7$ .

Objects shown in Figures 2 through 4 that do not appear in Figures 5 through 7 do not separate themselves from the stellar locus and thus can not be identified on the basis of their SDSS colors only. This includes metal-poor stars, Cepheids, and most asteroids.

However, as one can see from the figures, the CVs easily separate from the stellar locus, especially in the bluest colors. This is not that surprising, since a CV consists typically of a hot star, an accretion disk, and a cool star. The reddest objects are the longer period systems GK Per, SS Cyg, AE Aqr, and SS Aur, as well as the magnetic system AM Her in a low state. In all of these the red color is due to the contribution of the secondary star. At the same time the addition of a blue accretion disk/column separates them from the field stars. Most CVs occupy the region near (0,0) in all Sloan color-color plots, which is also

the area occupied by low redshift quasars (see Fig. 5) and white dwarfs (Fig. 4 of Lenz et al. 1998). Thus we expect new CVs and white dwarfs to be by-products of the quasar discoveries.

While in Figs. 5 and 6 all the points corresponding to RX And stand out from the stellar locus, in Fig. 7 we see that RX And at outburst is separable from the general stellar locus, but as the system returns to a quiescent state, its colors blend with the stellar locus in the  $i^*-z^*$  vs.  $r^*-i^*$  diagram.

Fig. 6 clearly shows that carbon stars separate from the stellar locus in  $r^*-i^*$  vs.  $g^*-r^*$ , more so at the reddest  $g^*-r^*$  colors. This is entirely in accord with synthetic photometry carried out by P. J. Green (private communication). Clearly, we need to observe more known dwarf carbon stars to see if they all have colors like G77-61 and LHS 1075, the colors of which are curiously identical within the errors. In any case, SDSS photometry will be effective for identifying carbon stars in the halo, although probably not for separating dwarfs from giants.

Since one of the primary goals of the Sloan project is to identify a very large number of quasar candidates, we naturally were interested in whether we managed to image any quasars serendipitously. As shown in Fig. 5, these would be objects that stand out from the stellar locus in the  $u^*-g^*$  vs.  $g^*-r^*$  diagram. In Table 6 we give photometry of 5 objects with  $u^*$  excesses. One of them, in fact, *is* a previously catalogued quasar. Near CM Del we imaged 2022+171 (= MG 2024+1717 = J202456.5+171814), a quasar of  $z = 1.05$ . Interestingly, it is at the same location in Fig. 5 as PG 2302+029, a quasar also of redshift 1.05, observed by Richards et al. (1997). Another blue object we serendipitously recovered is PB 7559 (Berger & Fringant 1984). To our knowledge there is no published spectrum; it could be a star or a quasar. The other three objects in our Table 6 are most likely stars, given their brightness.

Of the asteroids we observed, only one, 349 Dembowska, separates from the stellar locus (see Figs. 7 and 10). This is an R-type asteroid, notable for its *lack* of near infrared light, thus giving an  $i^*-z^*$  color that is “too blue”. From the spectra given by Xu et al. (1995), we expect that J-type and V-type asteroids will also stand out for the same reason.

In Figures 8, 9, and 10 we show photometry of the asteroids only. For reference, the colors of the Sun are also shown. Clearly, the C-type asteroids separate themselves from the other types of asteroids observed. This will allow us to identify C-type asteroids from SDSS photometry of moving objects.<sup>3</sup>

In Fig. 11 we show a color-magnitude diagram of the globular cluster M 15, where we have only plotted those points with Dophot internal errors (for each filter) less than 0.1 mag. M 15 has clearly identifiable blue horizontal branch (BHB) stars, located in Fig. 11 in the pentagonal box. The region of the RR Lyr stars would be just to the right. Since the RR Lyr stars are being observed at random phases in their pulsation cycles, we would expect these HB stars in the instability strip to show a wider spread in  $r^*$  than the BHB stars, and in fact they do show this.

It is worth commenting that the broadening of the lower giant branch is undoubtedly an artifact of crowding. As one approaches the frame limit, it becomes harder and harder to separate stars, especially in a globular cluster field. Therefore, if the counts from a given pixel in the frame are from two stars of comparable magnitude but widely varying colors, a “star” found by Dophot could be up to 0.75 mag “too bright”, with a color that

---

<sup>3</sup>We note that C-type asteroids are further subdivided into types B, F, and G depending on the near-ultraviolet light (Tholen & Barucci 1989, Fig. 5; Xu et al. 1995). The  $u^*-g^*$  colors of a large sample of C-type asteroids may allow further differentiation using SDSS data.

is considerably different than the colors of either star. And the photometry of this “star” could have an internal error less than our arbitrary limit of 0.1 mag.

We have identified 80 RR Lyr stars in our frames of M 15 using the list of coordinates given by Sawyer Hogg (1973). These stars have a median  $r^*$  magnitude of 15.76. The standard deviation of the distribution is  $\sigma_{r^*} = \pm 0.20$ . Silberman & Smith (1995) obtain a mean V magnitude for these stars of 15.82, adopt a mean absolute magnitude of  $\langle M_V \rangle = +0.36 \pm 0.12$ , color excess  $E(B-V) = 0.08$  mag, absorption  $A_V = 0.26$  mag, and therefore  $\log D(\text{pc}) = 4.04$ . Assuming an interstellar absorption law of the form  $A_\lambda \propto \lambda^{-1}$ , we find  $A_{r^*} = 0.23$  mag and  $\langle M_{r^*} \rangle = +0.33$ . (This could be slightly biased toward a value that is too bright because some of the stars may be blended with other stars.) Our data imply, however, that whatever the true mean absolute visual magnitude of the RR Lyr stars in M 15 (a matter of some debate), the mean absolute SDSS  $r^*$  magnitude of these stars is only slightly brighter.

We find that the BHB and RR Lyr stars in M 15 overlap the blue regions of the *entire* stellar locus in  $u^*-g^*$  vs.  $g^*-r^*$  and in  $i^*-z^*$  vs.  $r^*-i^*$ , but in Fig. 12 we show that they are found on a track parallel to our stellar locus, and on average 0.2 mag redder in  $r^*-i^*$  (or, equivalently, bluer in  $g^*-r^*$ ) in the  $r^*-i^*$  vs.  $g^*-r^*$  diagram. (A comparison of Figs. 5 and 12 shows that this is also where quasars and CVs are to be found.) Even if some of this displacement in  $r^*-i^*$  is attributable to an incorrect zero point in placing our Dophot output on our SDSS system, since so few field stars are this blue, it means that the identification of field BHB and RR Lyr stars from SDSS photometry is promising.

In Table 7 we give the median SDSS  $r^*$  magnitudes and colors of our sample of 143 BHB stars and 80 RR Lyr stars in M 15. We also include the median values for 247 BHB stars and 7 RR Lyr stars in M 2. We would expect that field BHB and RR Lyr stars found by SDSS in uncrowded fields would have colors within 0.2 mag of the values listed in Table

7 if their metallicities are comparable to those of the two clusters.

To investigate further the ability of SDSS to identify field RR Lyr stars in the northern Galactic cap, we have divided our data into three roughly equal area regions with galactic latitudes  $0 < |b| < 19^\circ$ ,  $19^\circ < |b| < 42^\circ$  and  $42^\circ < |b| < 90^\circ$ . We would expect the effects of interstellar reddening to affect the  $u^*-g^*$  vs.  $g^*-r^*$  stellar locus the most. In Fig. 13 we show that RR Lyr stars have colors that separate themselves from the general stellar locus *at higher galactic latitudes* (see lower set of points in the figure), where SDSS data will actually be obtained. Since the BHB stars have bluer  $g^*-r$  colors than RR Lyr stars, they are even further separated from the stellar locus at high galactic latitudes in the  $u^*-g^*$  vs.  $g^*-r^*$  diagram. Thus, we have confidence that SDSS will be able to identify many new BHB and RR Lyr candidates, and that the low latitude field stars present in this study, but not in SDSS, have not confused our conclusions.

We can use the information presented in Fig. 13 to investigate whether we can demonstrate any effects of interstellar reddening on SDSS colors. The upper set of 858 points (the stars at lower galactic latitudes) shows a wider locus of points than the lower set of 272 points. Is this just the effect of having a larger data set, putting a larger *number* of stars further from the mid-range, or do the distributions have different standard deviations? We begin by fitting an orthogonal regression line (also known as “Pearson’s major axis”) to each of the two stellar loci (Isobe et al. 1990). These are the lines that minimize the squares of the *perpendiculars* from the points to the lines. The two slopes are the same within the errors. The stars at lower galactic latitudes are displaced, on average, 0.039 mag to redder  $u^*-g^*$  colors, and are displaced 0.018 mag to redder  $g^*-r^*$  colors. These displacements, however, are not statistically significantly different than zero, given the uncertainties in the  $u^*-g^*$  intercepts of the plots.

If we now calculate, for each set of points, the RMS deviation from the respective

orthogonal regression line (i.e. perpendicular to the line), we find for the lower latitude sample  $\sigma_{\perp} = \pm 0.096$  mag, while for the higher latitude sample  $\sigma_{\perp} = \pm 0.066$  mag. The uncertainties of these standard deviations are  $\pm 0.002$  and  $\pm 0.003$ , respectively.<sup>4</sup> Thus, the *widths* of the distributions differ by roughly 10 times their uncertainties. The mid-latitude stars with  $19^{\circ} < |b| < 42^{\circ}$  give  $\sigma_{\perp} = \pm 0.081$  mag.

Another way of looking at the stellar locus according to ranges of galactic latitude is to pose the null hypothesis that the widths of the distributions shown in Fig. 13 are the same. Using a two sided F-test, we reject this null hypothesis at a 99.9 percent confidence level. Our data demonstrate that the stellar locus *is* widened by some combination of interstellar reddening and metallicity as we proceed from higher galactic latitudes to lower galactic latitudes.

#### 4. Conclusions

Using data provided by the Fermilab group for standards in common and graphs of the stellar locus (Newberg 1998, private communication), we have confirmed the position of the stellar locus in SDSS multi-color space found previously by Richards et al. (1997) and Newberg et al. (1997). Using our stellar locus, we have shown that cataclysmic variables, carbon stars, and R-type asteroids separate from the stellar locus on the basis of their SDSS colors. J-type asteroids, V-type asteroids, blue horizontal branch stars and RR Lyr stars should also be identifiable from SDSS photometry. C-type asteroids are

---

<sup>4</sup>The reader may recall that one can obtain an unbiased estimate of the variance ( $\hat{\sigma}^2$ ) of a distribution of points. An unbiased estimate of the variance of the variance is  $2(\hat{\sigma}^2)^2/(n-1)$ , where  $n$  is the sample size (Brownlee 1965). It can be shown that the *fractional* uncertainty of the RMS error of a distribution is  $\frac{1}{\sqrt{2(n-1)}}$ .

easily distinguishable from asteroids of type A, S, AS, and R on the basis of SDSS colors. However, Cepheids, metal-poor stars, and many types of asteroids do not separate from the stellar locus in color-color space, and thus cannot be identified on the basis of SDSS photometry alone.

We also provide a list of secondary stars that, after the completion of the SDSS photometric system, may be useful for calibrating future photometry. More observations of these stars should be obtained, and redder stars should also be observed.

KK thanks Hugh Harris of the US Naval Observatory for arranging the telescope time at the 1-m telescope and for observing assistance and advice; Alan Diercks, Scott Anderson, and Guillermo Gonzalez for data reduction advice; Doug Duncan for a list of metal-poor stars; George Wallerstein for information on globular clusters; Mark Hammergren for providing a list of coordinates of asteroids spanning the time of our observing run; and Heidi Newberg, Brian Yanny, Gordon Richards, and Steve Kent for useful discussions. Chris Stubbs provided much useful discussion and greatly appreciated moral and financial support. Useful information was obtained from Simbad, the astronomical data base of the Centre de Données astronomiques de Strasbourg.

## REFERENCES

- Berger, J., & Fringant, A.-M. 1984, *A&AS*, 58, 565
- Bothun, G., Elias, J. H., MacAlpine, G., Matthews, K., Mould, J. R., Neugebauer, G., & Reid, I. N. 1991, *AJ*, 101, 2220
- Brownlee, K. A. 1965, *Statistical Theory and Methodology in Science and Engineering* (New York: Wiley), on p. 300
- Deutsch, E. W. 1994, *PASP*, 106, 1134
- Fukugita, M., Ichikawa, T., Gunn, J. E., Doi, M., Shimasaku, K., & Schneider, D. P. 1996, *AJ*, 111, 1748 (F96)
- Green, P. J. 1998, in *The Carbon Star Phenomenon*, ed. R. F. Wing (Dordrecht: Kluwer), IAU Symposium 177, in press
- Green, P. J., & Margon, B. 1994, *ApJ*, 423, 723
- Gunn, J. E., & Knapp, G. R. 1993, in *Sky Surveys: Protostars to Protogalaxies*, ed. B. T. Soifer (San Francisco: Astronomical Society of the Pacific), 267
- Gunn, J. E., & Weinberg, D. H. 1995, in *Wide Field Spectroscopy and the Distant Universe*, eds. S. J. Maddox & A. Aragón-Salamanca (Singapore: World Scientific), pp. 3-14
- Hardie, R. H. 1962, in *Astronomical Techniques*, ed. W. A. Hiltner (Chicago: Univ. of Chicago Press), 178
- Harris, W. E. 1996, *AJ*, 112, 1487
- Kholopov, P. N. 1987, *General Catalogue of Variable Stars*, 4th ed., vol. III (Moscow: Nauka)
- Isobe, T., Feigelson, E. D., Akritas, M. G., & Babu, G. J. 1990, *ApJ*, 364, 104
- Krisciunas, K., et al. 1987, *PASP*, 99, 887

- Landolt, A. U. 1992, *AJ*, 104, 340
- Lee, P., et al. 1996, *Icarus* 120, 87
- Lenz, D. D., Newberg, H. J., Rosner, R., Richards, G. T., & Stoughton, C. 1998, *ApJS*, 119, in press
- Margon, B. 1998, *Phil. Trans. Roy. Soc. A*, in press (astro-ph/9805314)
- Margon, B., Aaronson, M., Liebert, J., & Monet, D. 1984, *AJ*, 89, 274
- Mateo, M. 1996, “Canary Islands Winter School 1996: Stellar Photometry Exercises Using DoPHOT”
- Newberg, H., Richards, G., Lenz, D., Fan, X., Richmond, M., & Yanny, B. 1997, *BAAS*, 29, 1385
- Richards, G. T., Yanny, B., Annis, J., Newberg, H. J. M., McKay, T. A., York, D. G., & Fan, X. 1997, *PASP*, 109, 39
- Sanduleak, N., & Pesch, P. 1988, *ApJS*, 66, 387
- Sawyer Hogg, H. 1973, *Publ. David Dunlap Obs.*, 3, No. 6
- Schechter, P., Mateo, M., & Saha, A. 1993, *PASP*, 105, 1342
- Silbermann, N. A. & Smith, H. A. 1995, *AJ*, 110, 704
- Slettebak, A., Keenan, P. C., & Brundage, R. K. 1969, *AJ*, 74, 373
- Tholen, D. J., & Barucci, M. A. 1989, in *Asteroids II*, eds. R. P. Binzel, T. Gehrels, & M. S. Matthews, (Tucson: Univ. of Arizona Press), 298
- Totten, E. J., & Irwin, M. J. 1998, *MNRAS*, 294, 1
- Warner, B. 1995, *Cataclysmic Variable Stars* (Cambridge: Cambridge Univ. Press)
- Xu, S., Binzel, R. P., Burbine, T. H., & Bus, S. J. 1995, *Icarus*, 115, 1

Table 1. Two Primary and 19 Secondary Standards<sup>a</sup>

Star Name	$r^*$	$u^*-g^*$	$g^*-r^*$	$r^*-i^*$	$i^*-z^*$	N	$n_u$	$n_{griz}$
BD +21° 607	9.12	0.89	0.28	0.10	−0.01	3	4	3
BD +17° 4708	9.35	0.92	0.29	0.10	0.02	5	5	5
SA 92-342	11.52	1.15	0.25	0.05	−0.03	6	11	6
SA 92-263	11.45	2.32	0.80	0.30	0.14	6	11	6
SA 94-242	11.72	1.23	0.10	−0.02	−0.06	6	12	8
SA 94-251	10.78	2.83	0.98	0.37	0.19	6	12	8
Ross 374	10.64	1.05	0.37	0.16	0.03	1	1	1
SA 95-218	11.89	1.49	0.49	0.16	0.04	6	12	7
SA 95-132	11.98	1.54	0.26	0.07	0.03	6	12	7
SA 95-142	12.74	1.33	0.43	0.16	0.05	6	12	7
SA 95-149	10.37	3.30	1.33	0.61	0.35	2	4	2
BD −21° 910	9.60	1.50	0.46	0.12	0.05	3	5	3
SA 110-499	11.38	2.11	0.82	0.46	0.31	5	9	7
SA 110-503	11.60	1.84	0.46	0.22	0.12	5	9	7
SA 110-441	10.99	1.32	0.37	0.11	0.03	2	6	4
SA 110-450	11.28	2.12	0.77	0.39	0.27	2	6	4
SA 112-805	12.17	1.24	−0.09	−0.14	−0.10	6	11	7
SA 112-822	11.22	2.34	0.80	0.28	0.13	6	11	7
SA 113-259	11.37	2.78	0.93	0.31	0.19	4	7	4
SA 113-260	12.29	1.27	0.31	0.05	0.00	4	7	4
BD +28° 4211	10.75	−0.52	−0.52	−0.38	−0.32	8	8	8

Table 1—Continued

Star Name	$r^*$	$u^*-g^*$	$g^*-r^*$	$r^*-i^*$	$i^*-z^*$	N	$n_u$	$n_{griz}$
-----------	-------	-----------	-----------	-----------	-----------	---	-------	------------

<sup>a</sup>N is the number of nights on which a given star was observed.  $n_u$  is the number of  $u^*$  frames obtained.  $n_{griz}$  is the number of frames obtained through the other four SDSS filters. The data for BD +17° 4708 are derived by Fukugita et al. (1996) from spectrophotometry.

Table 2. Observations of Cataclysmic Variables

Star Name	Type <sup>a</sup>	P <sup>b</sup>	JD–2450000	r <sup>*</sup>	u <sup>*</sup> –g <sup>*</sup>	g <sup>*</sup> –r <sup>*</sup>	r <sup>*</sup> –i <sup>*</sup>	i <sup>*</sup> –z <sup>*</sup>	n <sup>c</sup>
AR And	DN	3.9	726.8696	12.62	0.14	–0.18	–0.15	–0.13	1
RX And	DN	5.0	722.8987	11.34	0.06	–0.16	–0.12	–0.06	2
–	–	–	724.9118	12.07	0.09	–0.10	–0.01	–0.05	2
–	–	–	725.8525	12.47	0.07	–0.03	0.02	0.05	1
–	–	–	726.8532	13.08	0.09	0.03	0.17	0.12	1
V603 Aql	NL	3.3	722.6258	11.64	–0.15	–0.05	–0.12	–0.11	1
AE Aqr	IP	9.9	721.7215	10.74	1.18	0.68	0.24	0.10	1
FO Aqr	IP	4.9	720.7041	13.48	–0.19	0.01	–0.12	–0.14	1
TT Ari	NL	3.3	723.9725	11.16	0.05	–0.21	–0.20	–0.15	2
SS Aur	DN	4.4	718.9606	14.85	–0.34	0.48	0.48	0.36	1
V425 Cas	NL	3.6	726.6912	15.24	0.13	0.02	–0.09	–0.07	1
SS Cyg	DN	6.6	719.6611	11.55	0.33	0.61	0.31	0.14	1
–	–	–	725.6642	11.50	0.38	0.56	0.32	0.20	1
–	–	–	726.6522	11.53	0.30	0.57	0.34	0.17	1
CM Del	NL	3.9	722.6347	14.18	0.10	0.01	–0.01	–0.05	1
AM Her	AM	3.1	719.6168	14.68	0.00	0.53	0.83	0.84	2
V1159 Ori	DN	1.5	720.9754	13.59	0.25	–0.15	–0.17	–0.13	1
LS Peg	NL	4.2	720.6713	11.92	0.04	–0.03	–0.16	–0.15	1
GK Per	IP	47.9	720.0037	12.44	0.87	0.82	0.38	0.25	1
AO Psc	IP	3.6	721.7065	13.62	–0.16	–0.09	–0.13	–0.02	1

Table 2—Continued

Star Name	Type <sup>a</sup>	P <sup>b</sup>	JD–2450000	r <sup>*</sup>	u <sup>*</sup> –g <sup>*</sup>	g <sup>*</sup> –r <sup>*</sup>	r <sup>*</sup> –i <sup>*</sup>	i <sup>*</sup> –z <sup>*</sup>	n <sup>c</sup>
-----------	-------------------	----------------	------------	----------------	--------------------------------	--------------------------------	--------------------------------	--------------------------------	----------------

<sup>a</sup>DN = dwarf nova; NL = nova-like; AM = polar; IP = intermediate polar.

<sup>b</sup>P is the orbital period of the system in hours.

<sup>c</sup>n is the number of 5 filter data sets obtained. Some extra u<sup>\*</sup>-band images were also obtained.

Table 3. Observations of Carbon Stars<sup>a</sup>

Star Name	r*	u*–g*	g*–r*	r*–i*	i*–z*	N	n <sub>u</sub>	n <sub>griz</sub>
C01	13.18	2.99 ± 0.01	1.33	0.43	0.38	1	2	1
C02	15.43	2.83 ± 0.03	1.12	0.32	0.29	2	4	4
C03	15.25	3.07 ± 0.02	1.13	0.32	0.26	1	2	1
C07	13.99		2.48	0.91	0.55	1	0	1
C08	14.66	2.80 ± 0.04	1.36	0.40	0.38	1	2	2
C09	14.40	4.70 ± 0.13	1.61	0.60	0.50	1	2	2
C10	15.15	3.25 ± 0.02	1.25	0.38	0.35	2	4	3
C13	18.10	1.09 ± 0.04	0.45	0.25	−0.03	1	2	2
C15	10.10	3.85 ± 0.01	1.75	0.59	0.56	1	3	1
C23	14.71	2.57 ± 0.04	0.90	0.21	0.22	1	2	2
C26	14.19	3.51 ± 0.02	1.35	0.39	0.41	2	2	2
C30	13.42	6.06 ± 0.32	1.78	0.55	0.48	1	1	1
C31	13.99		2.00	0.75	0.50	1	0	1
CLS 105	13.96	2.35 ± 0.01	0.97	0.27	0.14	1	2	2
CLS 112	14.63	1.94 ± 0.01	0.79	0.19	0.13	1	2	2
G77-61	13.20	3.00 ± 0.01	1.53	0.40	0.15	2	4	3
LHS 1075	14.34	3.02 ± 0.04	1.54	0.40	0.20	2	5	3
SKB2	11.96	2.09 ± 0.01	0.79	0.19	0.12	1	2	2
BD −19° 132	10.26	3.75 ± 0.01	1.35	0.38	0.37	1	2	1
AM Scl	12.02	5.74 ± 0.15	1.84	0.70	0.43	1	2	2

Table 3—Continued

Star Name	$r^*$	$u^*-g^*$	$g^*-r^*$	$r^*-i^*$	$i^*-z^*$	N	$n_u$	$n_{griz}$
BD $-19^\circ$ 290	10.57	$3.05 \pm 0.01$	1.10	0.29	0.32	1	2	1

<sup>a</sup>Objects prefixed by a “C” are from Bothun et al. (1991); CLS objects are from Sanduleak & Pesch (1988); for G77-61 and LHS 1075 see Deutsch (1994); for the last four objects in the table see Slettebak, Keenan & Brundage (1969). N is the number of nights on which a given star was observed.  $n_u$  is the number of  $u^*$  frames obtained on which the object was detected with an adequate S/N ratio.  $n_{griz}$  is the number of frames obtained through the other four SDSS filters.

Table 4. Observations of Asteroids<sup>a</sup>

No.	Name	Type	1997 Date	UT	r*	u*–g*	g*–r*	r*–i*	i*–z*	n
446	Aeternitas	A	30 Sep	11:09	14.33	1.54	0.61	0.26	0.12	1
702	Alauda	C	30 Sep	11:47	12.75	1.58	0.45	0.13	0.03	1
82	Alkmene	S	28 Sep	10:57	12.43	1.71	0.64	0.18	–0.05	1
–	–	–	3 Oct	10:56	12.27	1.70	0.60	0.21	–0.07	2
774	Armor	S	28 Sep	03:52	12.97	1.68	0.71	0.15	0.06	1
–	–	–	4 Oct	03:23	13.21	1.78	0.65	0.23	–0.02	2
371	Bohemia	AS	4 Oct	05:05	12.64	1.77	0.65	0.21	–0.04	2
349	Dembowska	R	29 Sep	11:54	10.28	1.92	0.70	0.15	–0.22	1
433	Eros <sup>b</sup>	S	30 Sep	12:26	13.30	1.94	0.67	0.24	–0.07	2
480	Hansa	S	29 Sep	09:59	12.25	1.74	0.63	0.22	–0.07	1
10	Hygeia	C	28 Sep	12:05	11.43	1.56	0.46	0.10	0.02	1
683	Lanzia	C	1 Oct	03:35	14.23	1.53	0.48	0.13	0.04	1
–	–	–	3 Oct	05:01	14.21	1.62	0.45	0.14	–0.02	1
68	Leto	S	27 Sep	10:37	10.11	1.76	0.66	0.18	0.03	1
149	Medusa	S	29 Sep	06:12	12.57	1.82	0.68	0.22	–0.01	1
196	Philomela	S	28 Sep	08:51	11.41	1.81	0.64	0.19	–0.03	1
314	Rosalia	C	5 Oct	03:15	13.95	1.57	0.46	0.10	0.00	2
138	Tolosa	S	5 Oct	04:11	11.57	1.94	0.69	0.17	–0.01	2

<sup>a</sup>With one exception the Universal Time given corresponds to the r\* image, or the mean of two r\* images. n is the number of full 5 filter data sets obtained.

Table 5. Observations of Metal-Poor Stars and Cepheids<sup>a</sup>

Star Name	[Fe/H]	Per(d)	r*	u*–g*	g*–r*	r*–i*	i*–z*
Metal-poor stars:							
BD +72° 94	–1.80		9.83	0.94	0.26	0.08	0.02
HD 16031	–2.20		9.67	0.99	0.24	0.06	0.04
BD +3° 740	–2.90		9.68	0.90	0.30	0.07	0.02
G 186-26	–2.80		10.74	0.85	0.23	0.07	–0.01
BD –17° 6036	–2.80		10.22	1.52	0.64	0.30	0.11
BD +38° 4955	–2.50		10.80	1.04	0.51	0.22	0.08
Cepheids:							
M2-V1		15.583	12.76	1.70	0.56	0.09	0.19
M2-V5		17.606	13.12	1.92	0.72	0.23	0.14
M2-V6		19.295	12.79	1.11	0.45	0.11	0.07
M2-V11		67.0	11.64	1.35	0.43	0.11	0.10
M15-V1		1.438	15.18	1.34	0.29	0.17	0.06

<sup>a</sup>The periods of the Cepheids were taken from Sawyer Hogg (1973).

Table 6. Field Objects with  $u^*$  Excesses

Identification	$\alpha$ (2000)	$\delta$ (2000)	$b^a$	$r^*$	$u^*-g^*$	$g^*-r^*$	$r^*-i^*$	$i^*-z^*$
2022+171	20:24:50.0	+25:00:24	−7.6	15.11	0.53	0.02	−0.10	0.06
	20:24:56.6	+17:18:13	−12.0	17.81	0.33	0.20	0.02	0.01
	20:25:11.5	+25:05:45	−7.6	15.17	0.40	0.07	−0.04	0.03
PB 7559	23:04:22.1	+53:18:45	−6.1	16.19	0.40	0.26	0.13	−0.01
	23:07:51.1	−13:40:28	−62.7	18.03	0.25	0.03	−0.02	−0.11

<sup>a</sup>Galactic latitude in degrees.

Table 7. Blue Horizontal Branch and RR Lyrae Stars (median values)

Cluster	[Fe/H] <sup>a</sup>	Star Type	n	$r^*$	$u^*-g^*$	$g^*-r^*$	$r^*-i^*$	$i^*-z^*$
M 15	−2.22	BHB	143	15.99	1.33	−0.06	0.02	−0.08
—	—	RR Lyr	80	15.76	1.27	0.19	0.16	−0.02
M 2	−1.62	BHB	247	16.28	1.13	−0.09	−0.12	−0.05
—	—	RR Lyr	7	15.88	1.17	0.24	0.06	0.03

<sup>a</sup>Metallicity is taken from Harris (1996).

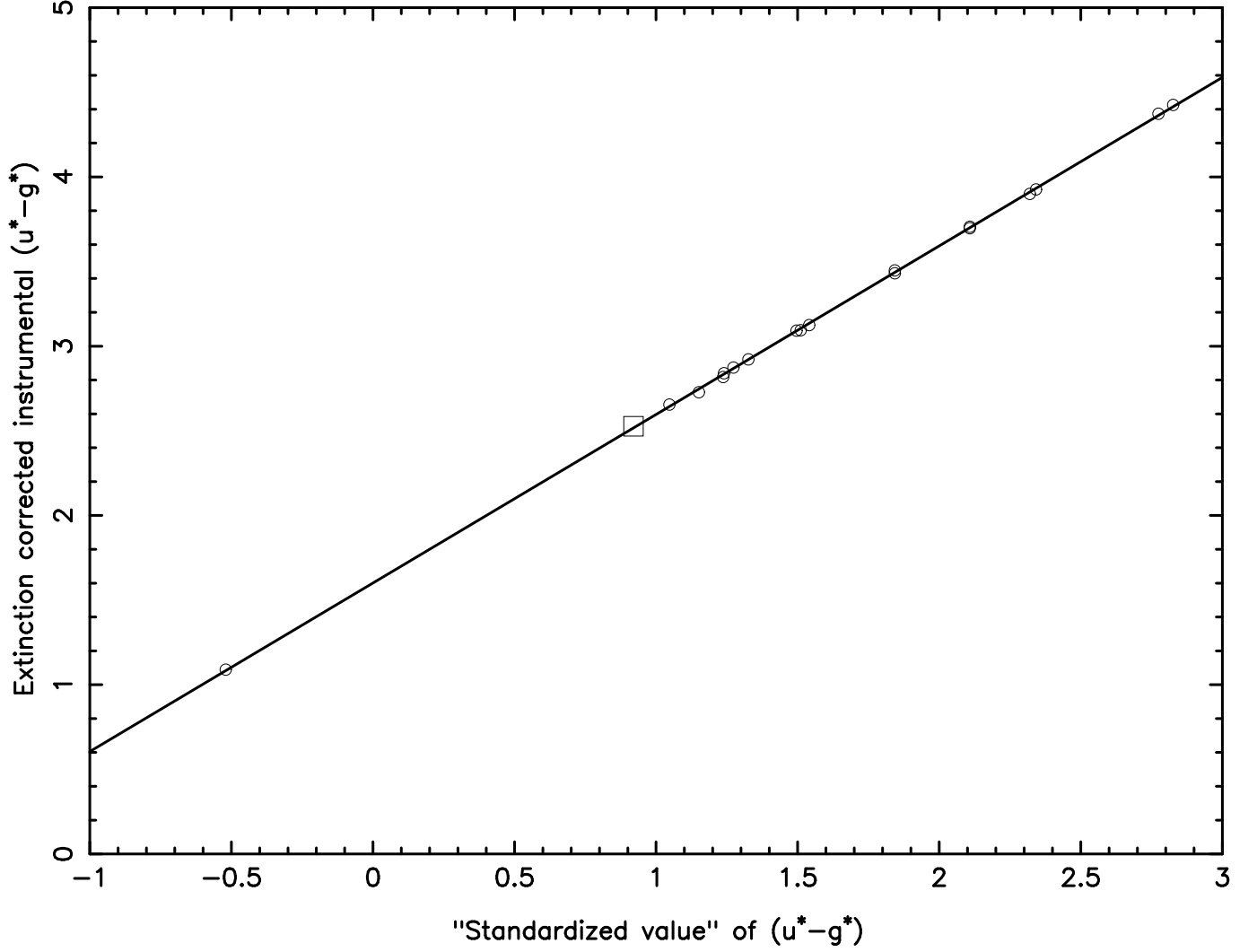


Fig. 1.—  $u^*-g^*$  photometric solution for 29 September 1997 UT. The  $y$ -intercept is the “photometric zero point” for this color for this night. The slope of the line is not statistically different than 1.00. The RMS residual of the fit is  $\pm 0.010$  mag. The open square represents the primary standard BD +17° 4708. The smaller open circles represent secondary standards.

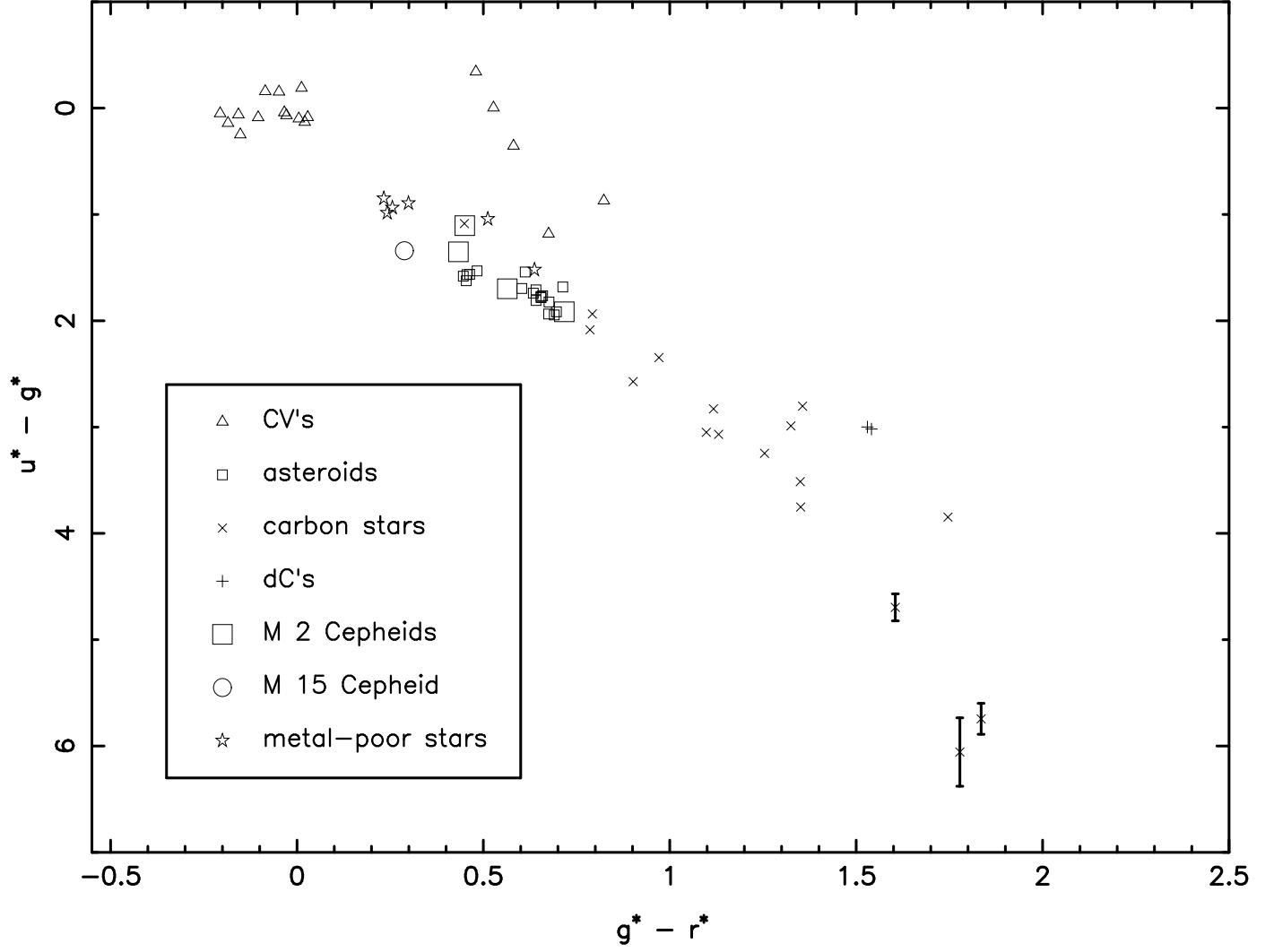


Fig. 2.—  $u^* - g^*$  vs.  $g^* - r^*$  data for program objects from Tables 2 through 5. The point for SS Cyg is the average of 3 nights of data. Some carbon star points are the averages of 2 nights of data. Other points represent nightly averages.

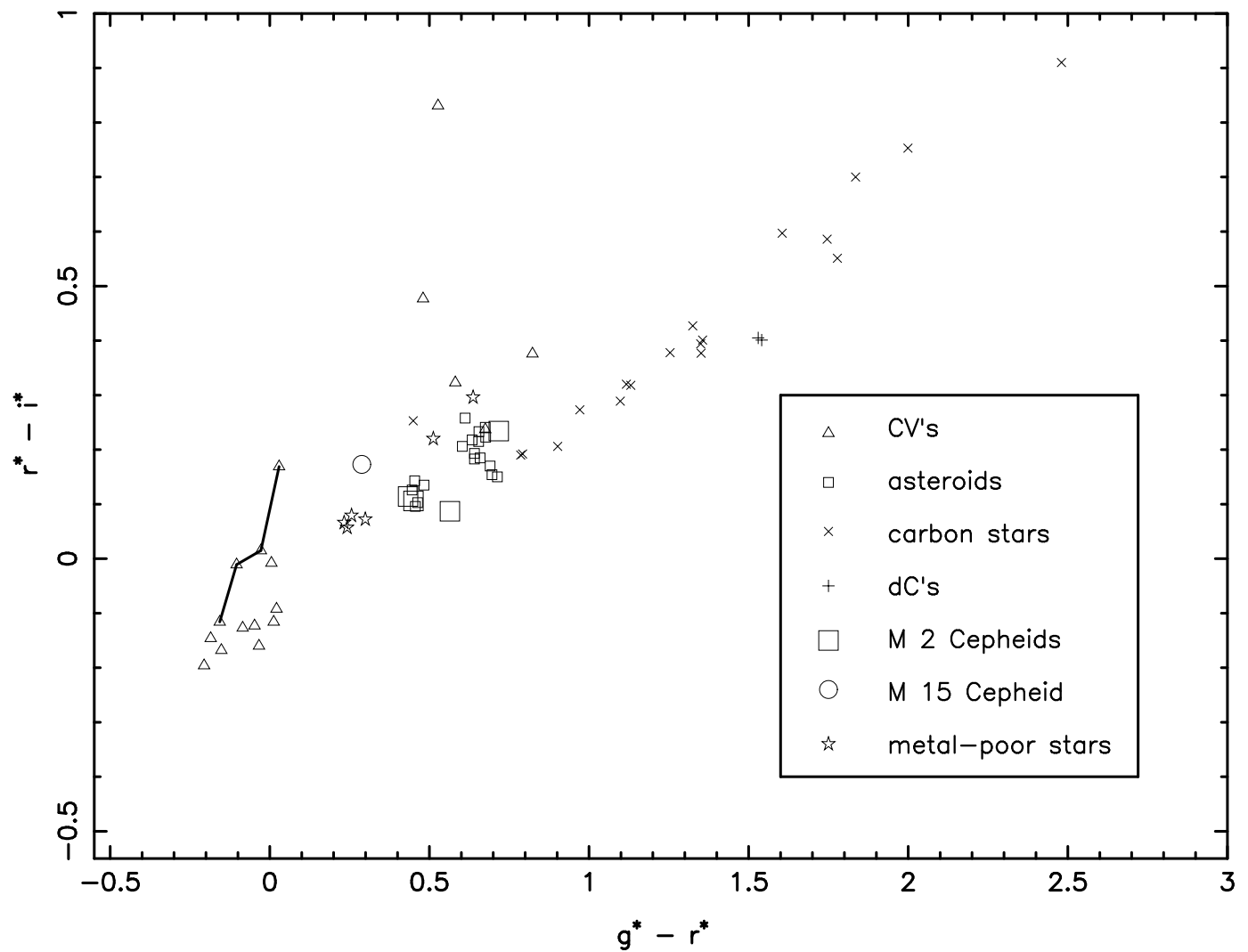


Fig. 3.—  $r^* - i^*$  vs.  $g^* - r^*$  data for program objects from Tables 2 through 5. The triangles connected by a line are data of four separate nights for RX Andromedae, which was recovering from an outburst.

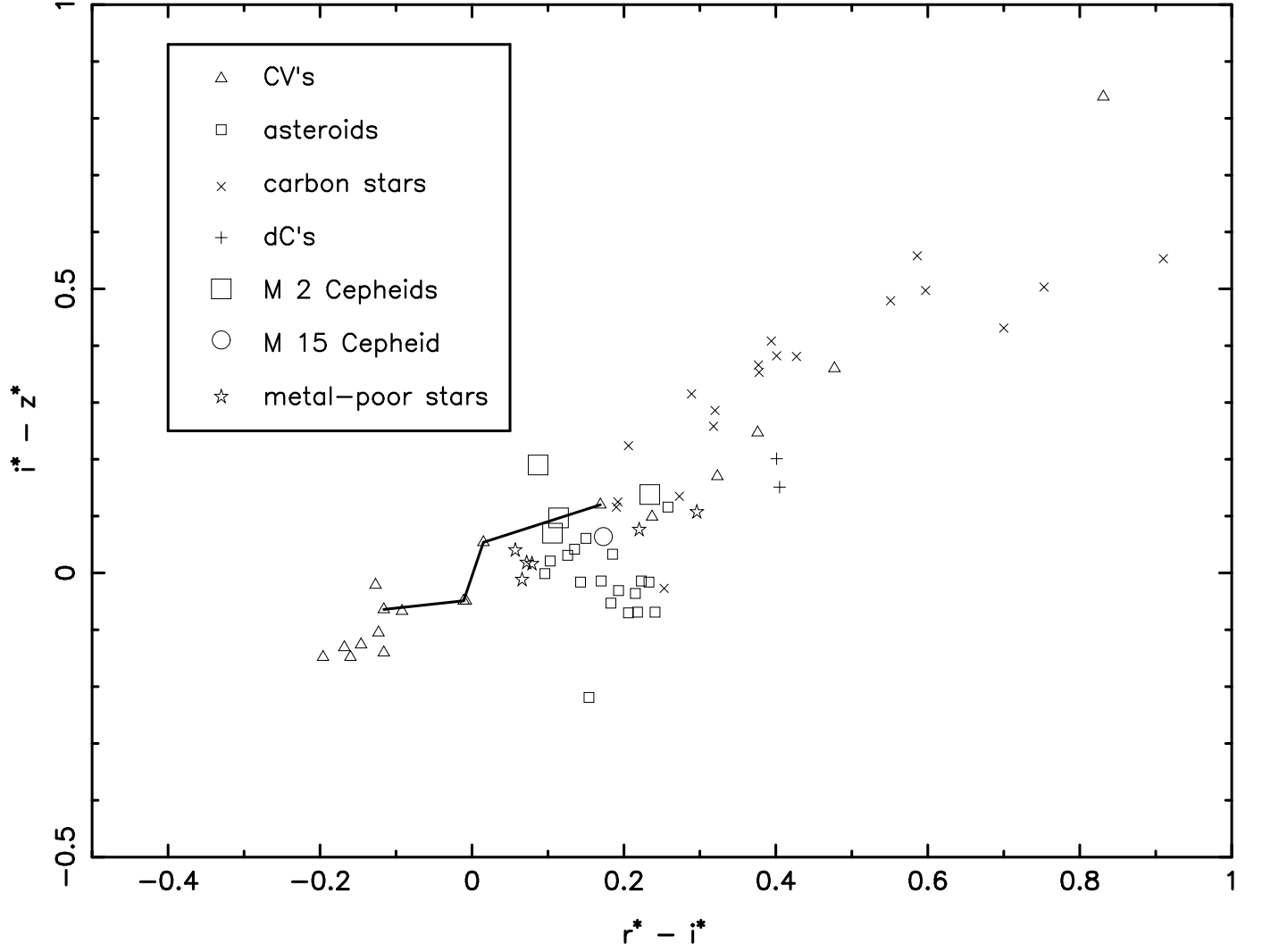


Fig. 4.—  $i^* - z^*$  vs.  $r^* - i^*$  data for program objects from Tables 2 through 5. The triangles connected by a line are data of four separate nights for RX Andromedae, which was recovering from an outburst.

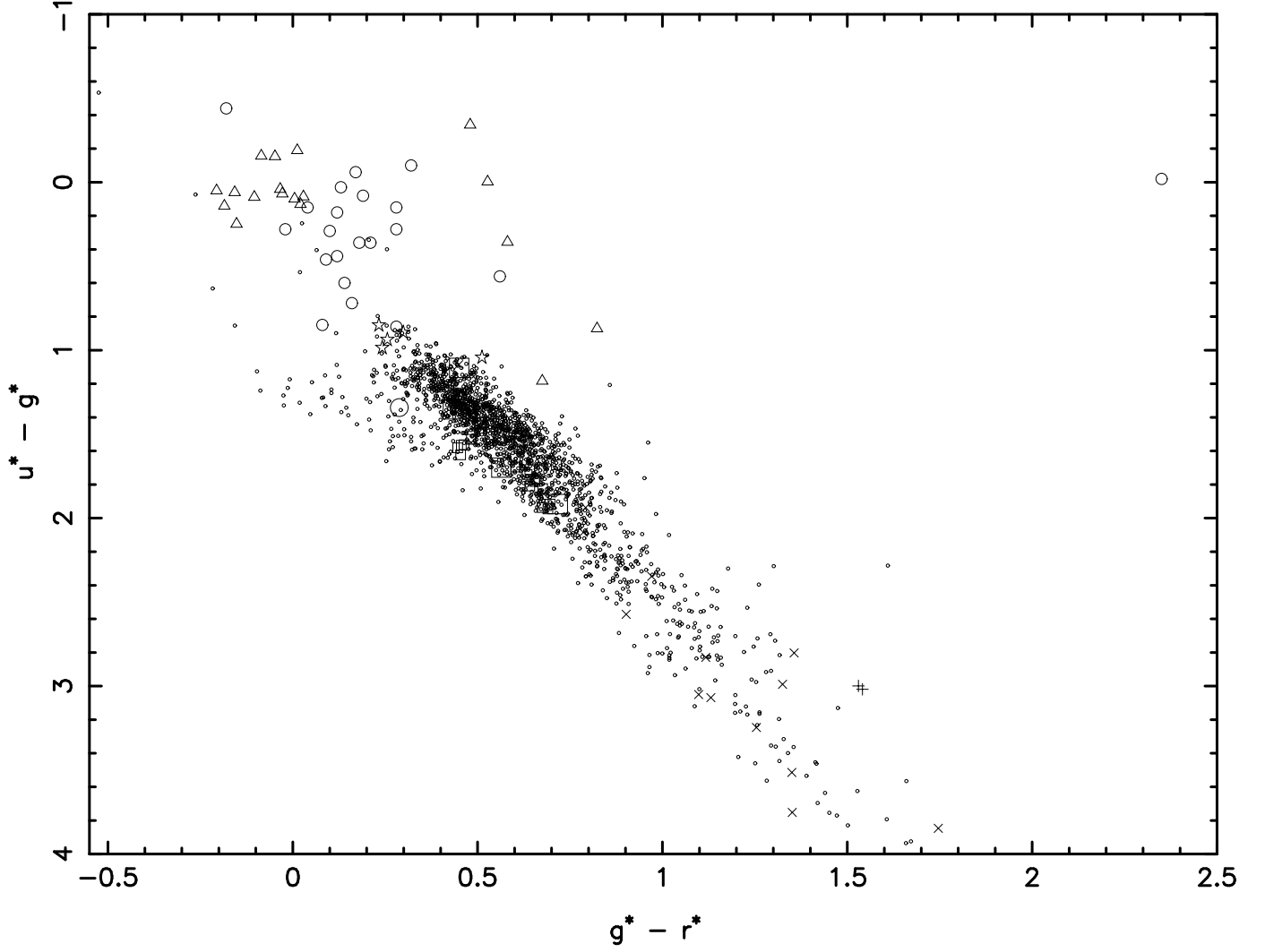


Fig. 5.—  $u^* - g^*$  vs.  $g^* - r^*$  data for program objects, quasars, and the stellar locus obtained from roughly 80 fields at a variety of galactic latitudes. Symbols are the same as in Figs. 2 to 4, plus these additional ones: tiny dots represent field stars, and smaller open circles represent quasars from Richards et al. (1997), with redshifts ranging from 0.06 to 2.72. The three carbon stars reddest in  $u^* - g^*$  are off the bottom of the plot. Only 2 field stars are observed to have  $u^* - g^* > 4.0$ .

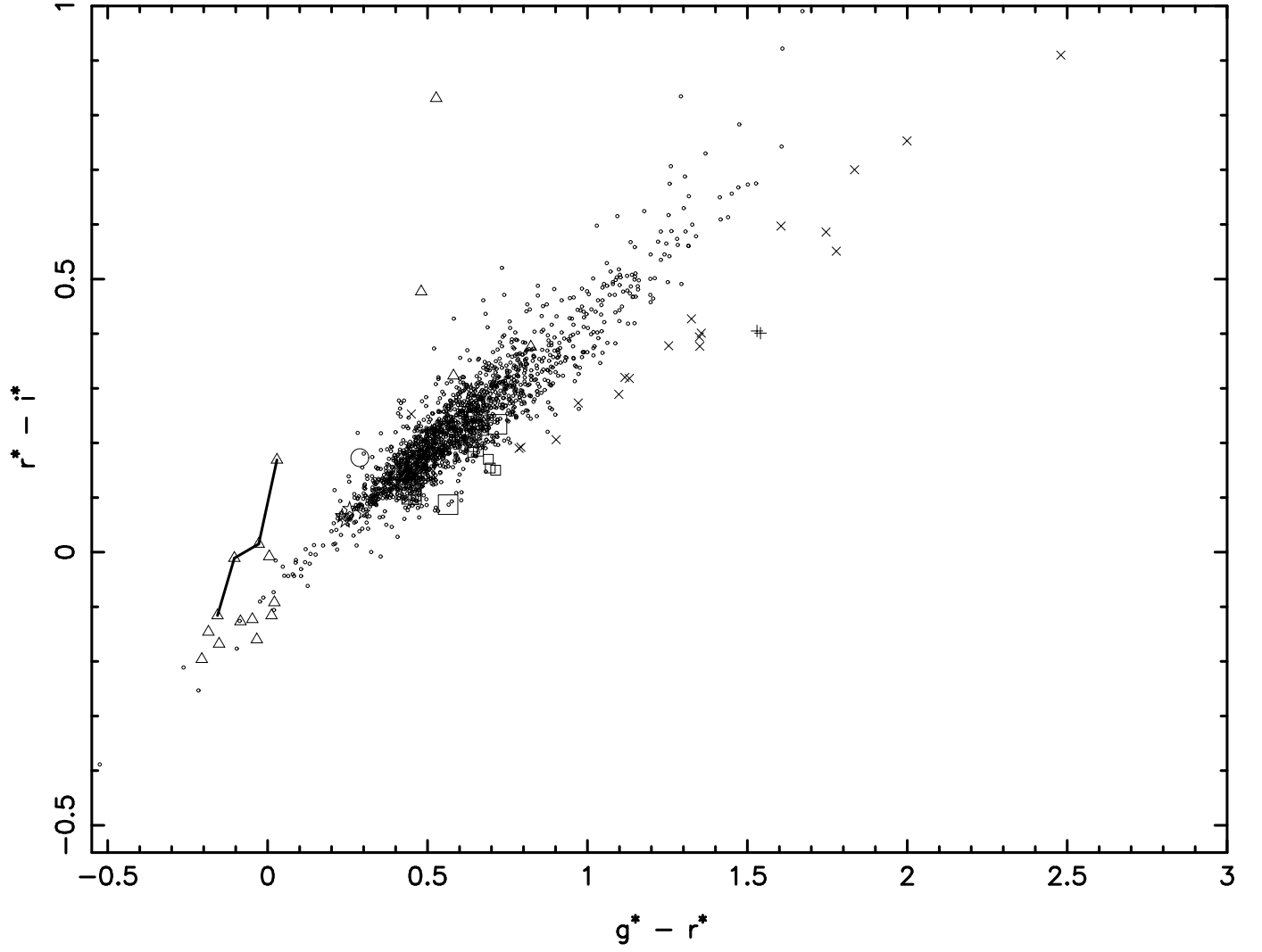


Fig. 6.—  $r^* - i^*$  vs.  $g^* - r^*$  data for program objects and field stars. Symbols are the same as in Fig. 5.

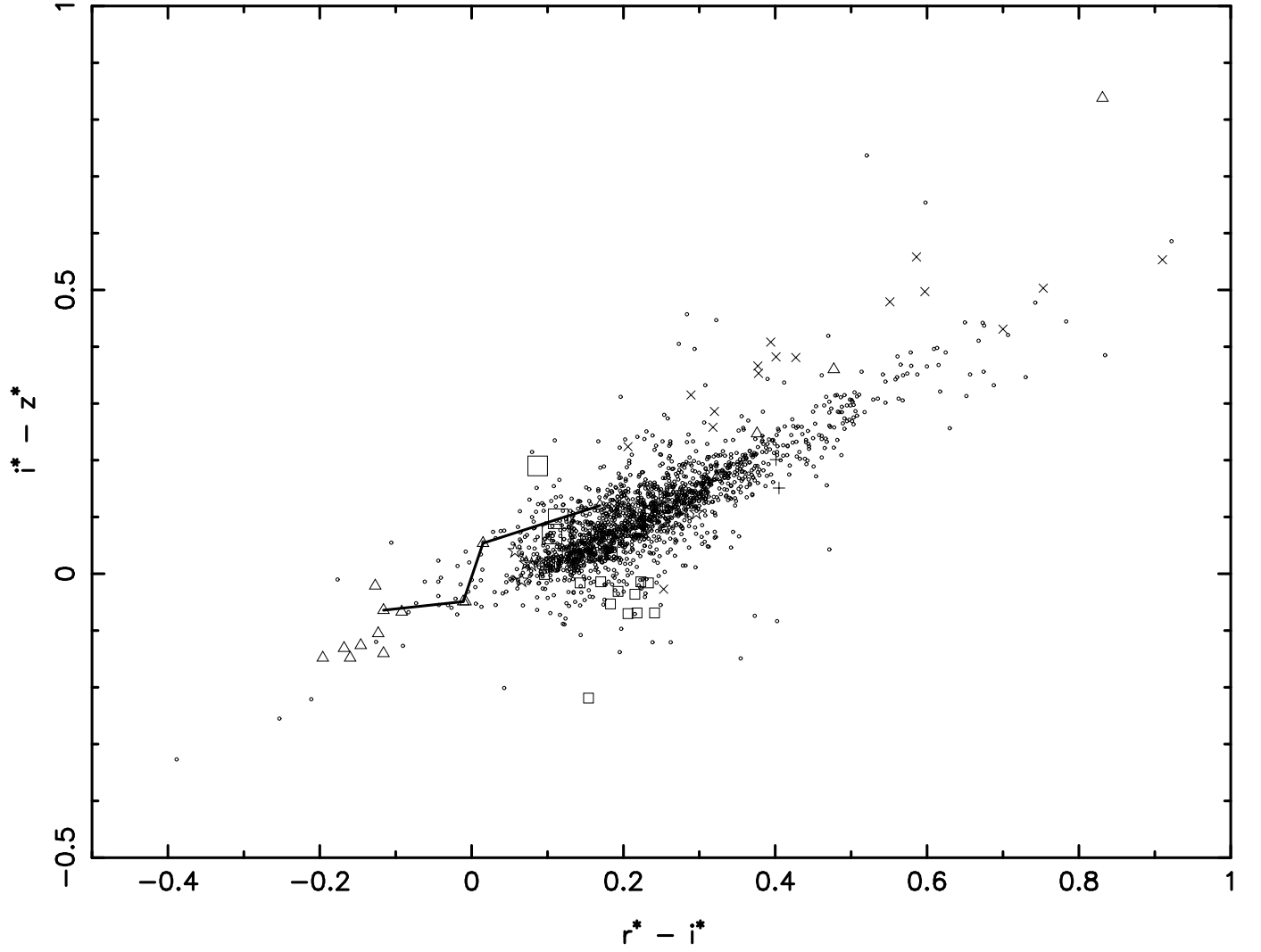


Fig. 7.—  $i^* - z^*$  vs.  $r^* - i^*$  data for program objects and field stars. Symbols are the same as in Fig. 5.

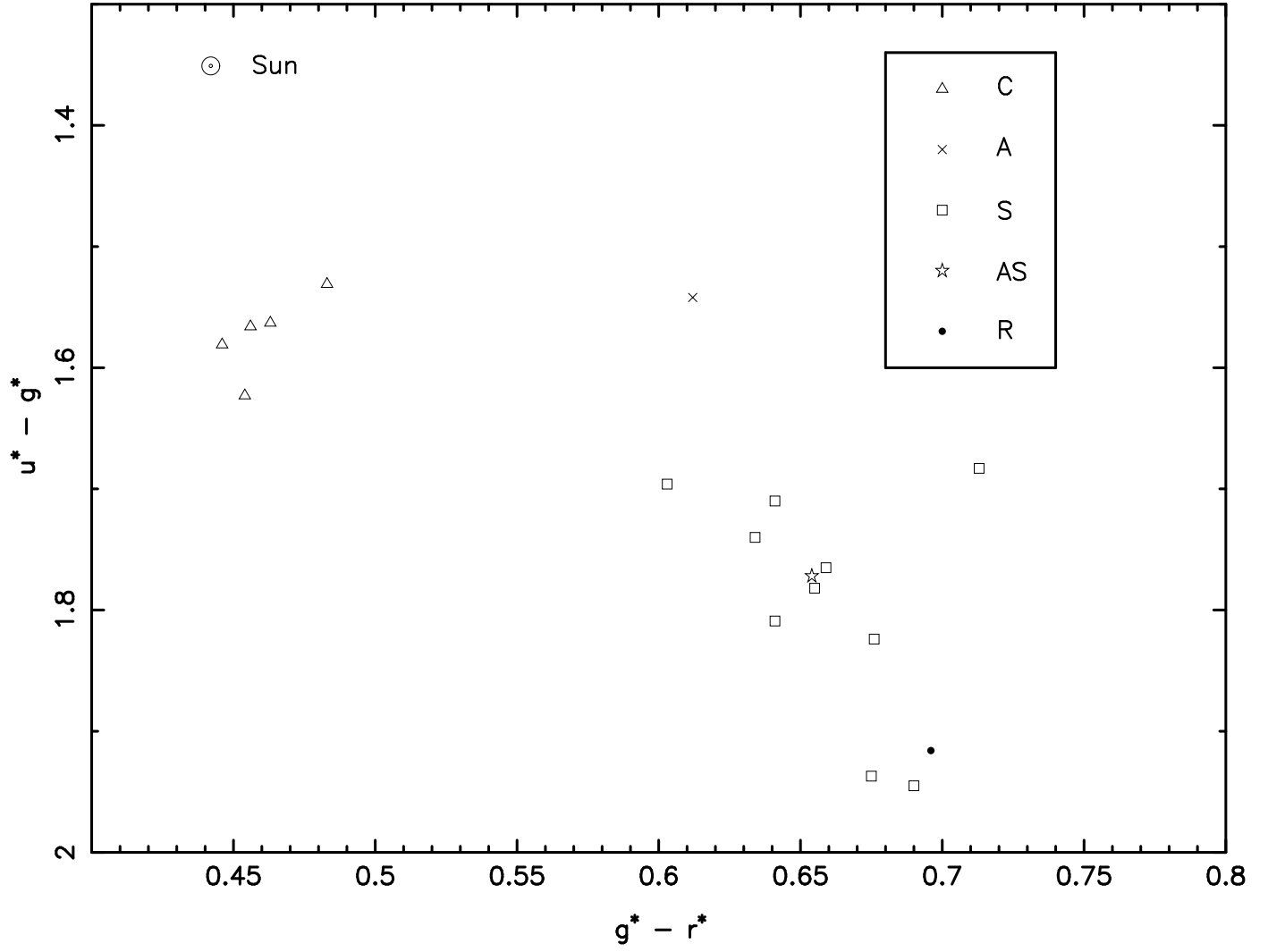


Fig. 8.—  $u^* - g^*$  vs.  $g^* - r^*$  data for asteroids. Three asteroids were measured on more than one night. We plot all nightly means.

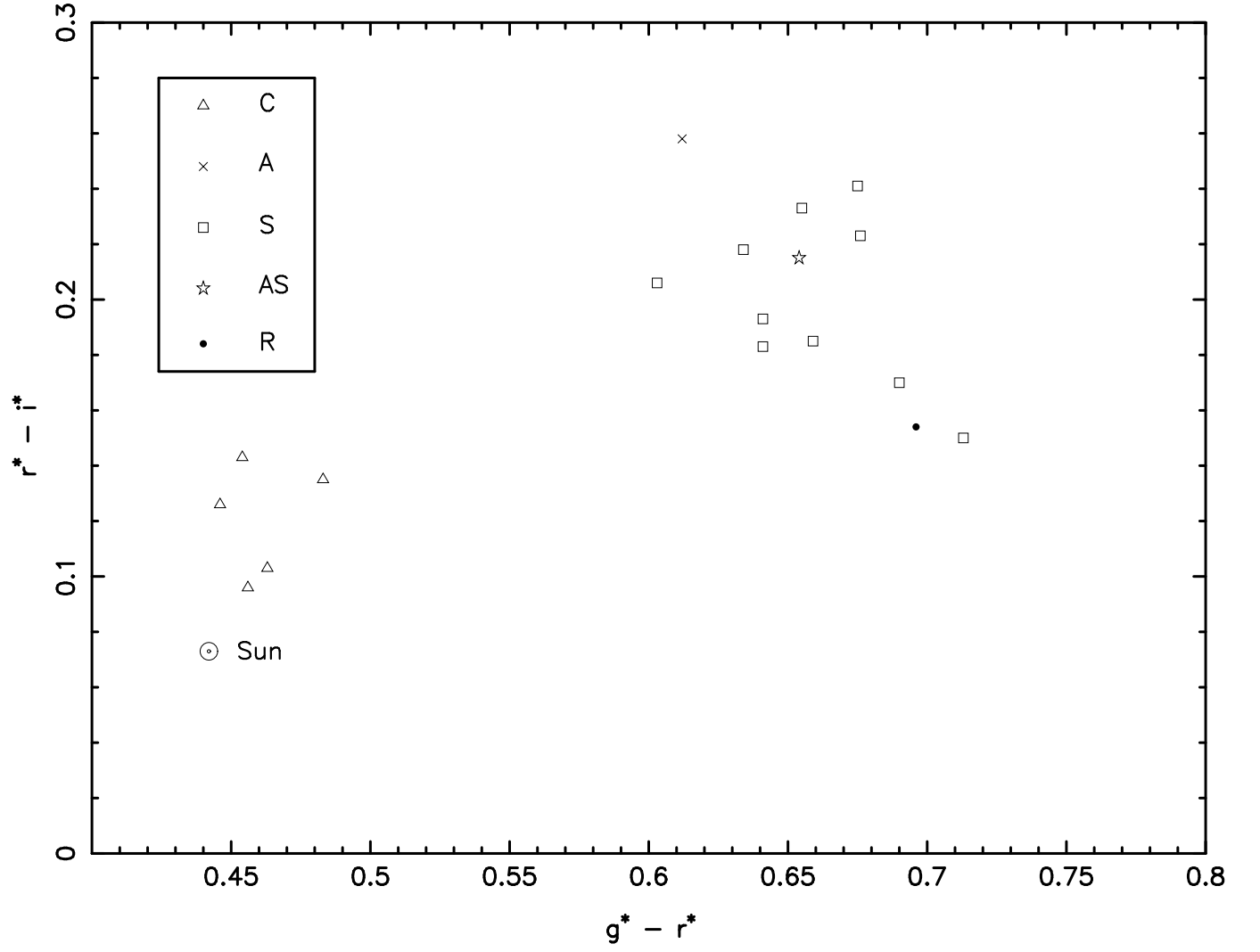


Fig. 9.—  $r^* - i^*$  vs.  $g^* - r^*$  data for asteroids.

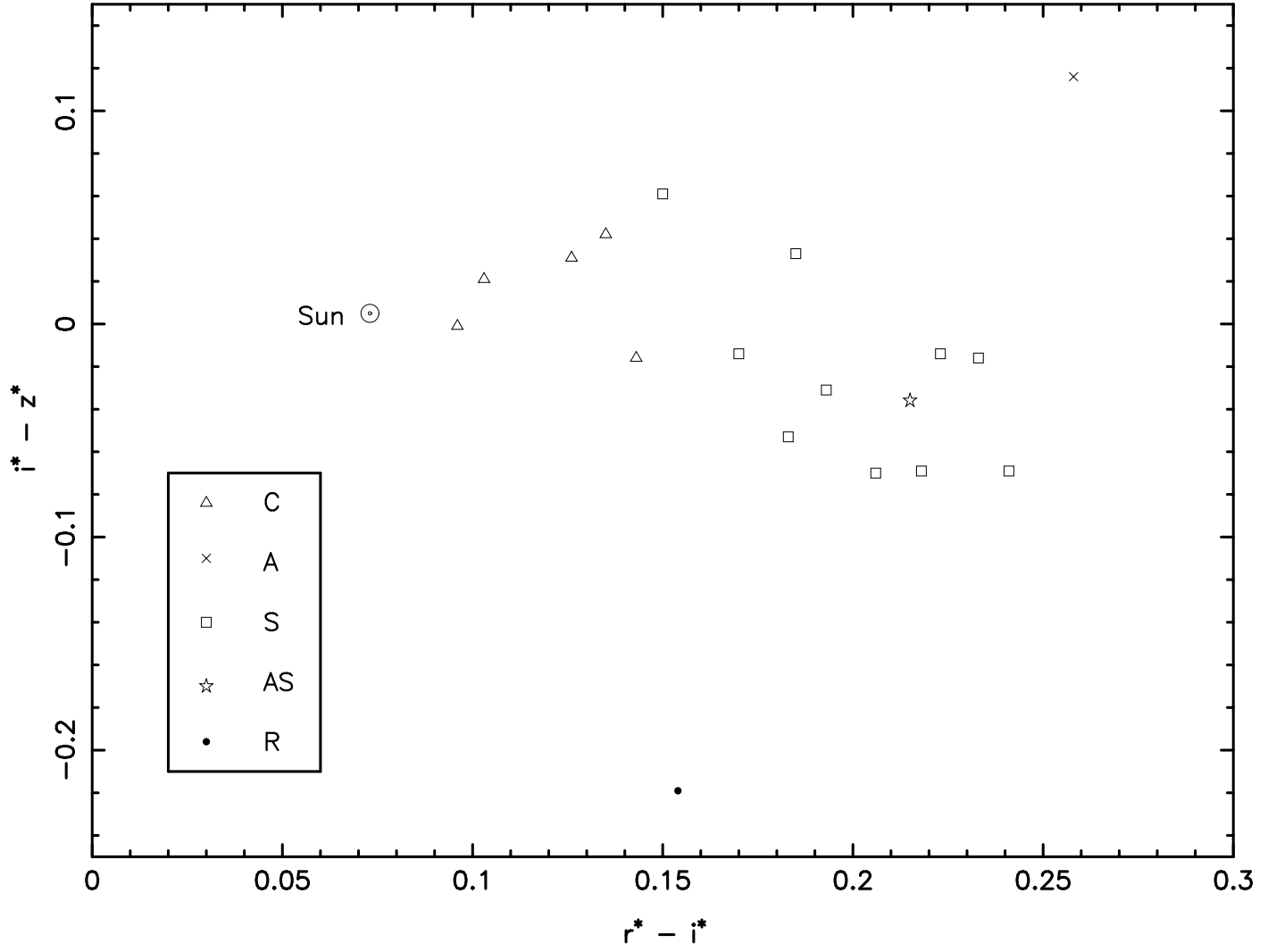


Fig. 10.—  $i^* - z^*$  vs.  $r^* - i^*$  data for asteroids.

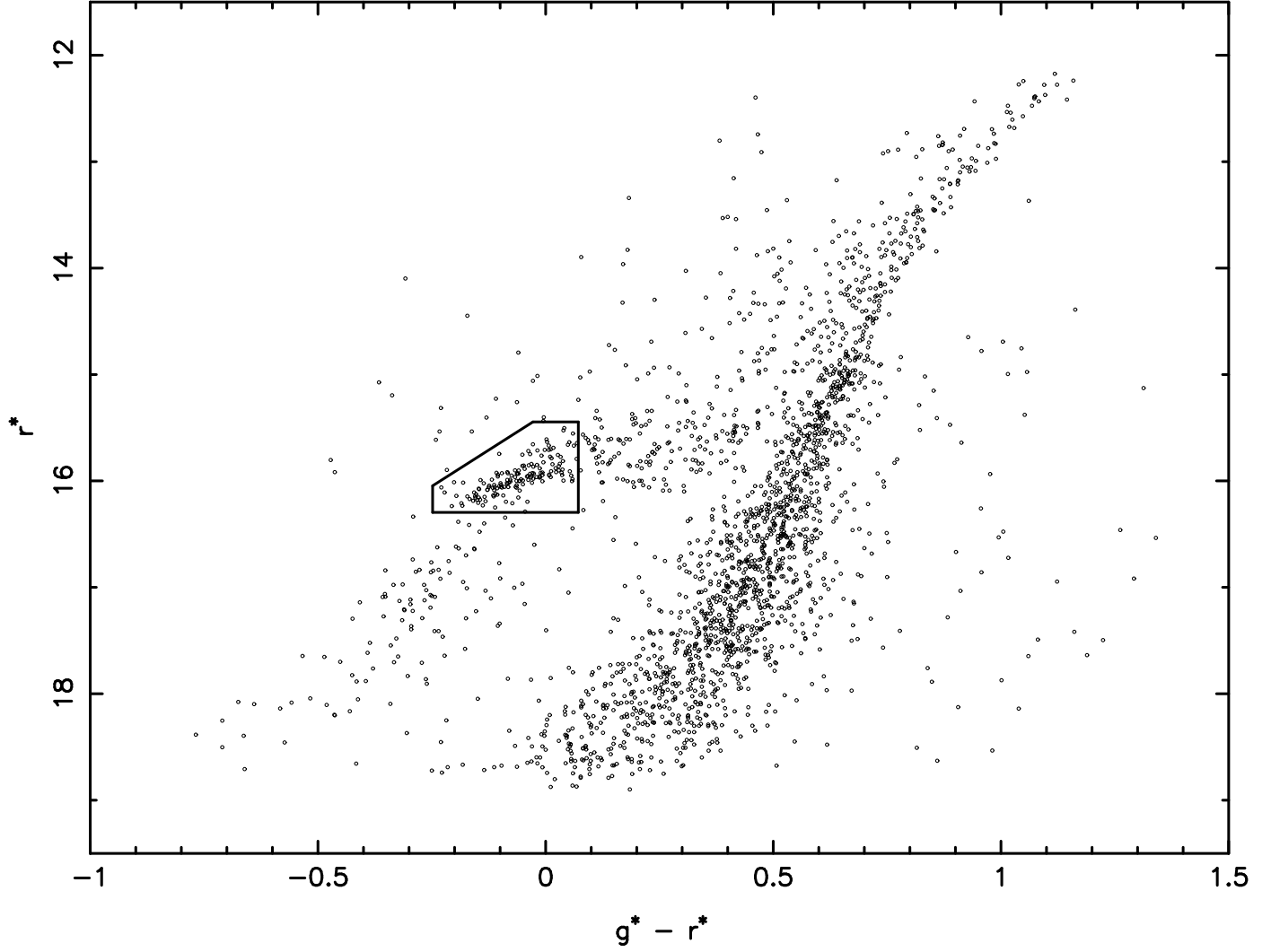


Fig. 11.— Color-magnitude diagram for the globular cluster M 15. The blue horizontal branch stars are located in the pentagonal box. Some RR Lyr stars are found in this box, but most are found in a region of comparable size just to the right of the box, and slightly higher.

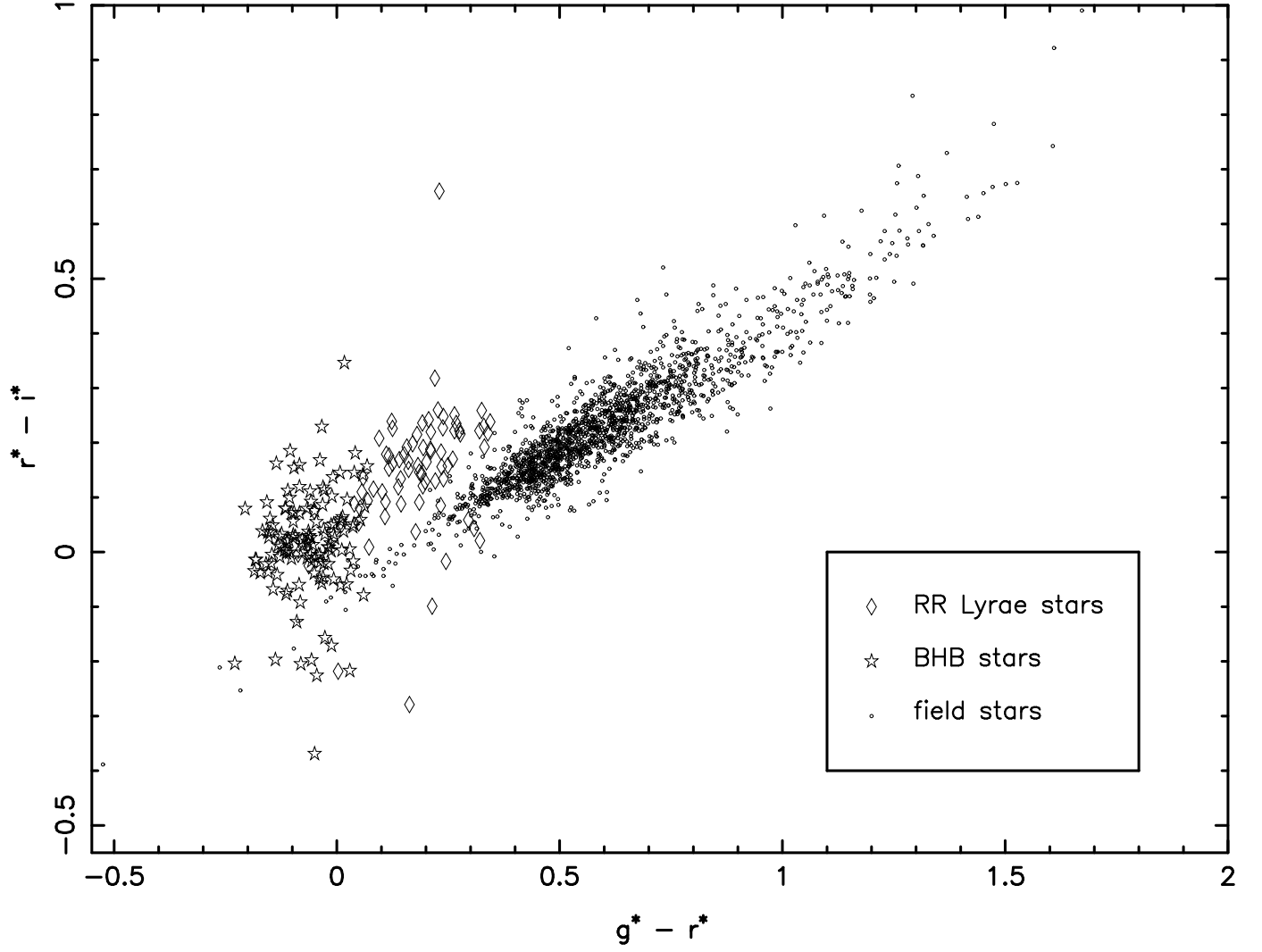


Fig. 12.—  $r^* - i^*$  vs.  $g^* - r^*$  data for M 15 stars. RR Lyr stars were identified using the coordinates given by Sawyer Hogg (1973). Outliers are most likely due to the effect of crowding discussed in the text.

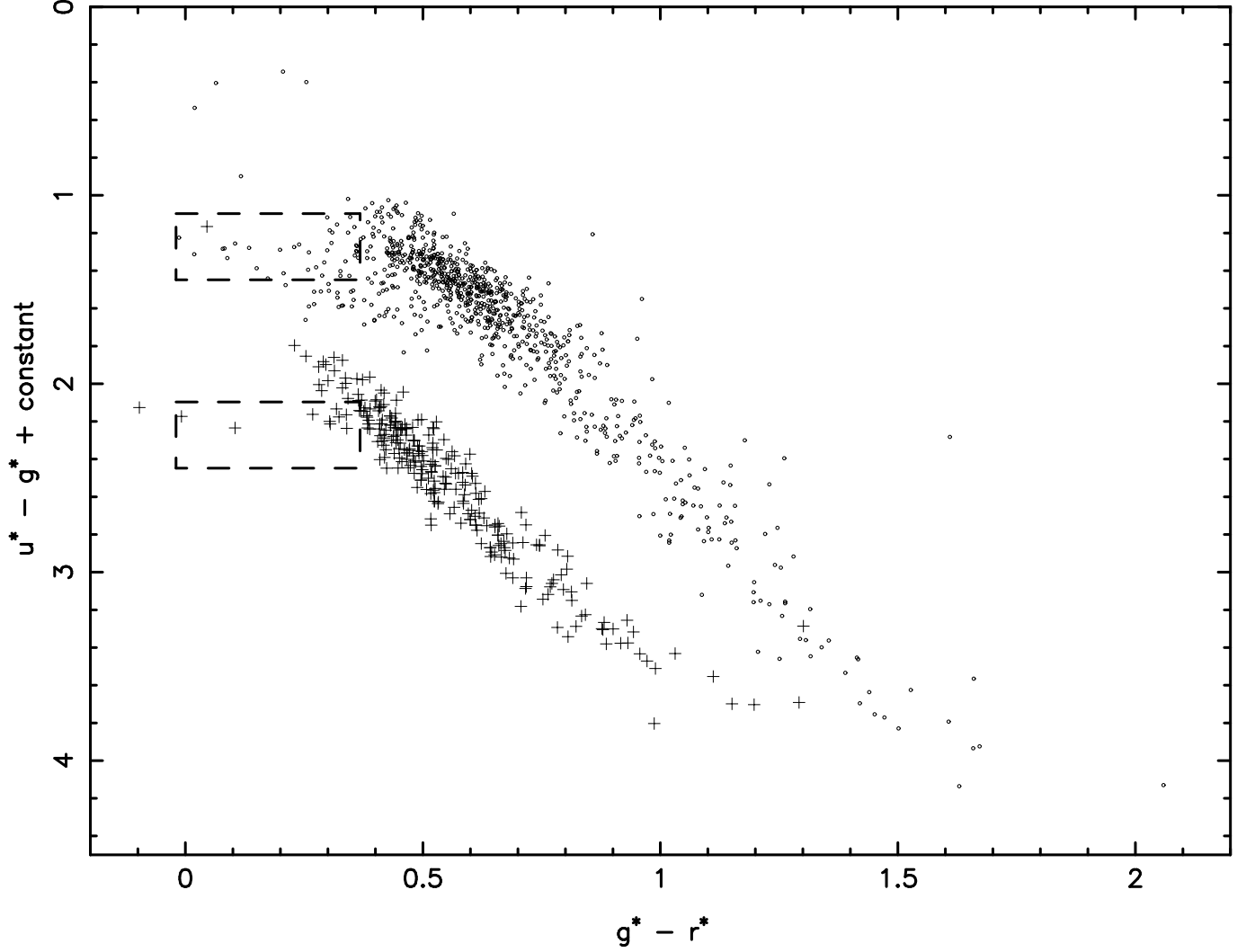


Fig. 13.—  $u^*-g^*$  vs.  $g^*-r^*$  stellar locus for field stars with galactic latitude  $0^\circ < |b| < 19^\circ$  (dots) and with  $42^\circ < |b| < 90^\circ$  (pluses). The lower set of points has been offset by +1.00 mag in  $u^*-g^*$  for the purpose of display. The boxes indicate the location of RR Lyr stars in M 15 ( $\pm 2\sigma$  from mean value in each direction). The BHB stars are located to the left of the boxes.